ENVIRONMENTAL ENGINEERING SCIENCE
Volume 31, Number 7, 2014

DOI: 10.1089/ees.2013.0473

Nanostructured Graphene-Titanium Dioxide Composites Synthesized by a Single-Step Aerosol Process for Photoreduction of Carbon Dioxide

Wei-Ning Wang, Yi Jiang, John D. Fortner, and Pratim Biswas*

Department of Energy, Environmental, and Chemical Engineering, Washington University in St. Louis, St. Louis, Missouri.

Received: November 26, 2013 *Accepted in revised form: March 22, 2014*

Abstract

Photocatalytic reduction of carbon dioxide (CO_2) to hydrocarbons by using nanostructured materials activated by solar energy is a promising approach to recycling CO_2 as a fuel feedstock. CO_2 photoreduction, however, suffers from low efficiency mainly due to the inherent drawback of fast electron-hole recombination in photocatalysts. This work reports the synthesis of nanostructured composites of titania (TiO_2) nanoparticles (NPs) encapsulated by reduced graphene oxide (rGO) nanosheets via an aerosol approach. The role of synthesis temperature and TiO_2/GO ratio in CO_2 photoreduction was investigated. As-prepared nanocomposites demonstrated enhanced CO_2 conversion performance as compared with that of pristine TiO_2 NPs due to the strong electron trapping capability of the rGO nanosheets.

Key words: carbon neutrality; crumpling; photocatalysis; solar energy; spray pyrolysis

Introduction

Fossil fuel-based power generation is widely considered a major source of carbon dioxide (CO_2) emissions to the atmosphere (Biswas *et al.*, 2011). Several strategies to combat rising CO_2 emissions are being researched. For example, CO_2 capture and sequestration (CCS) has been proposed as a viable approach for this purpose (Metz *et al.*, 2005). However, CCS technology is plagued by requirements of high energy inputs and costs, making it economically challenging for widespread adoption. Furthermore, the approach has not been widely demonstrated, and until such studies are done, large-scale adoption will be limited.

Another effective approach to counter CO_2 emissions is to convert them to value-added products, such as hydrocarbon fuels, which not only mitigates CO_2 emissions but also recycles it as a fuel feedstock. However, due to the stability of CO_2, it is difficult to reduce or convert it to other hydrocarbons. The production of syngas, a mixture of carbon monoxide (CO) and hydrogen (H_2), through reforming of methane ($CO_2 + CH_4 \rightarrow 2CO + H_2$), provides a potential pathway for large-scale CO_2 capture and utilization (Song, 2006). This reaction, however, is endothermic and requires high temperatures (700–900°C) for the reaction to proceed.

Alternately, photocatalysis-based technologies may be a more desirable way to convert CO_2 into valuable chemicals, as it utilizes inexpensive co-reactants such as water in conjunction with abundant renewable solar energy. The promise of developments in nanotechnology makes this approach a potentially feasible one. In a typical semiconductor-based photocatalyst system, light with energy equal to or higher than the bandgap of the semiconductor results in photoexcitation and transfer of the electron (e^-) to the conduction band, leaving a hole (h^+) in the valence band. Ideally, after photoexcitation, the e^-–h^+ pairs (or excitons) should be separated spatially through built-in potentials and transferred to redox active sites, which involves several critical charge transfer steps (Fujishima *et al*., 2008). Among them, the e^-–h^+ recombination is considered one of the major limiting steps, as it is two or three orders of magnitude faster than other electron transfer processes (Indrakanti *et al*., 2009). Therefore, any process that inhibits e^-–h^+ recombination would greatly increase the efficiency and improve the rates of CO_2 photoreduction.

A widely accepted method that is used to slow down the e^-–h^+ recombination rate is to deposit metal nanoparticles (NPs), such as platinum, copper, or iron, on semiconductor surfaces (Tseng *et al.*, 2004; Usubharatana *et al.*, 2006; Indrakanti *et al.*, 2009; Wang *et al.*, 2012a). These metal NPs serve as electron sinks and, thus, separate the e^-–h^+ pair to enhance the photoreduction efficiency. They usually need to be carefully engineered to get a better control over particle size, purity, and distribution, which require additional and often complex synthesis steps. In particular, the continued use of these metal-modified photocatalysts is limited due to photoinduced coagulation of these metal NPs (Eckstein and Kreibig, 1993; Kimura, 1994), resulting in increased particle size and deterioration in performance.

**Corresponding author:* Department of Energy, Environmental, and Chemical Engineering, Washington University in St. Louis, St. Louis, MO 63130. *Phone:* +1-314-935-5548; *Fax:* +1-314-935-5464; *E-mail:* pbiswas@wustl.edu

Interestingly, graphene nanosheets have emerged as a promising candidate for this purpose, as they are excellent conductors and can act as electron sinks to increase the lifetime of the photoinduced e^-–h^+ pairs. Graphene nanosheets also have a large specific surface area that could enhance the absorption of light and adsorption of reactants to further improve the CO_2 photoreduction performance. In addition, such nanosheets exhibit high flexibility, enabling the possibility of encapsulation to form composite materials for a variety of applications (Kamat, 2011). However, the flat morphology of graphene sheets can be problematic, as the strong van der Waals attraction between layers can lead to aggregation and reduction of effective surface area (Luo *et al.*, 2011). One possible solution is to turn the two-dimensional (2D) nanosheets into three-dimensional crumpled balls by aerosol techniques (Luo *et al.*, 2011; Wang *et al.*, 2012b). Crumpling the flat morphology of graphene oxide (GO) nanosheets enables the harnessing of the large specific surface area without compromising the desirable electrical properties (Stankovich *et al.*, 2006; Ma *et al.*, 2012). The relationship between the evaporation rate and confinement force in the crumpling process via aerosol routes has been investigated systematically (Wang *et al.*, 2012b).

This work reports the development of crumpled nanocomposites of titania (TiO_2) NPs encapsulated by reduced graphene oxide (rGO) nanosheets using a single-step furnace aerosol reactor (FuAR) method, which features short processing time and easy scalability. Effects of synthesis temperature and TiO_2/GO ratio on the CO_2 photoreduction efficiency were investigated systematically. The reduction mechanisms of GO played an important role in CO_2 photoreduction. The comparison between the two reduction methods, thermal reduction and simultaneous photoreduction of GO is reported.

Materials and Methods

GO synthesis

The modified Hummers method was used to make GO from graphite (Hummers, 1958; Wang *et al.*, 2012b). First, graphite powder (45 μm; Sigma-Aldrich) was oxidized with potassium permanganate in the presence of sulfuric acid (H_2SO_4) at 0°C. The solution was then allowed to slowly warm to room temperature. It was then stirred at 35°C for 2 h, after which the suspension was cooled in an ice bath and diluted with deionized (DI) water. To ensure the complete reduction of residual permanganate to soluble manganese ions, 30% hydrogen peroxide was added until gas evolution ceased. The suspension was finally filtered and washed with DI water until no presence of H_2SO_4 was detected. The GO was dried at 50°C overnight to obtain a brownish-black powder. To prepare the GO aqueous solution, the GO powder was dissolved in water and sonicated for 1 h. Finally, the solution was centrifuged at 10,000 rpm for 30 min to obtain the supernatant—a stable suspension of GO nanosheets in water (Model 5804, Eppendorf AG, Hamburg, Germany).

GO-TiO_2 nanocomposite preparation

Nanocomposites were prepared by using the FuAR method (Fig. 1a). Details of the method are described in our previous reports (Wang *et al.*, 2011, 2012b). The precursor solution was made by mixing TiO_2 NPs (Aerodisp® W 740 X, Evonik Degussa Corp.), GO suspension, and DI water at various ratios. The solution was loaded into a collison nebulizer (BGI, Inc.). Compressed nitrogen (N_2) gas entered through an inlet valve at a controlled pressure of 96.5 kPa, traveled into the nebulizer, and atomized the solution into micrometer-sized droplets ($d_{droplet} = 2.8\ \mu$m) (Wang *et al.*, 2012b). The droplets passed through the furnace in which solvent (i.e., water in this work) evaporation, nanosheets crumpling, and composite particle formation occurred. The procedure was repeated by varying the furnace synthesis temperature (200–1000°C, at 5 wt% TiO_2) and the weight percentages of TiO_2 (relative to GO) in solution (0–20 wt%, at 800°C).

Material characterization

The hydrodynamic particle size and zeta potential of the precursors (aqueous suspensions of TiO_2 NPs and GO nanosheets) were measured by a dynamic light scattering (DLS) method using a Zetasizer Nano ZS system (Malvern Instruments Ltd.) with a measurable size range from 0.3 nm to 10 μm.

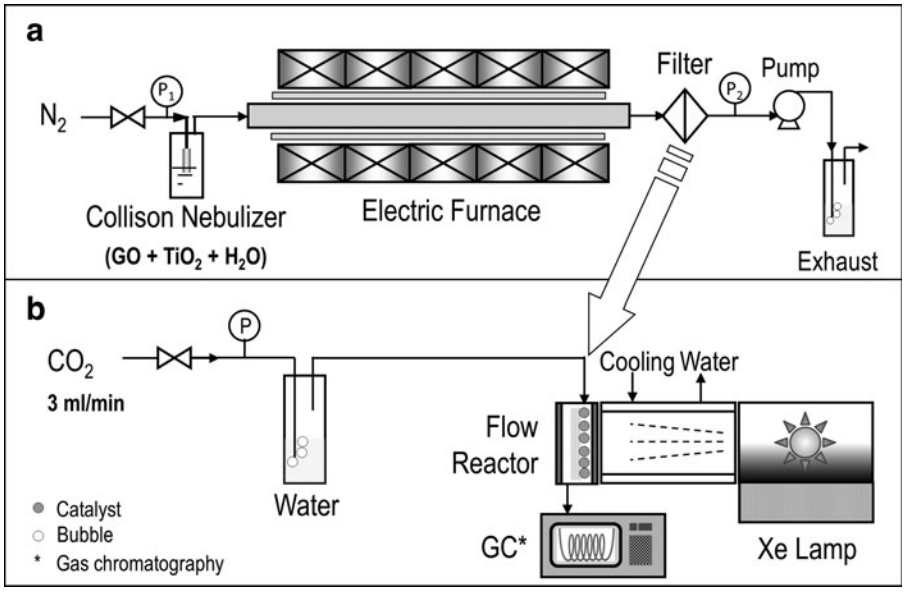

FIG. 1. Schematic diagram of experimental setup. **(a)** Furnace aerosol reactor for nanocomposite preparation. **(b)** Carbon dioxide (CO_2) photoreduction analysis systems.

Table 1. Characterization of Precursors in Graphene Oxide–Titania Mixture

Sample no.	*TiO_2 weight percentage (wt%)*	*Hydrodynamic diameter, d_p (nm)*	*PDI (–)*	*Zeta potential of mixture (mV)*	*Zeta potential of TiO_2 (mV)*
01	0	293.4	0.276	–33.6	NA
02	5.0	2207	0.597	–23.2	–24.9
03	10.0	3180	1.000	–15.3	–22.6
04	15.0	5055	0.495	–15.6	–25.6
05	20.0	11,620	0.928	–14.7	–25.7

GO mass concentration was fixed at 0.54 mg/mL, which was determined by UV-VIS measurements (Wang *et al.*, 2012b).
PDI, the polydispersity index, a dimensionless measure of the broadness of the size distribution (ISO 13321, 1996); GO, graphene oxide; TiO_2, titania.

A red laser ($\lambda = 633$ nm) was used as the light source with a scattering angle of 90°. The morphology of product particles (dry nanocomposites) were examined using field emission scanning electron microscopy (Nova NanoSEM 230, FEI Co.) operated at 10 kV. The inner structure of the films was analyzed by transmission electron microscopy (TEM; Tecnai™ G^2 Spirit, FEI Co.). Surface properties were analyzed by a Laser Raman spectrometer (Kaiser HoloLab 5000) with a laser wavelength of 520 nm. Five points of each sample were analyzed, and the average intensities were used as final results.

CO_2 photoreduction analysis

The photoreduction analysis system was detailed in our previous papers (Wang *et al.*, 2011, 2012a) and is briefly described here (Fig. 1b). Compressed CO_2 gas was used as the carbon source. It passed through a water bubbler and generated a mixture of CO_2 and water vapor. The gaseous mixture was then fed into a continuous flow reactor in which the photocatalysts were loaded. The reactor is cylindrical in shape with a quartz window vertically facing the light source, which is a xenon (Xe) lamp operated at 450 W with an accumulated intensity of 19.6 mW/cm^2 in the effective UV range (250–388 nm). Before each test, the reactor loaded with samples was first purged with CO_2 and water vapor at 100 mL/min for 1 h and then, the flow rate was reduced and maintained at 3 mL/min during the test. The concentrations of effluent gases as a function of irradiation time were recorded automatically by the gas chromatography (GC) through an automated gas valve, using helium as the carrier gas. The GC

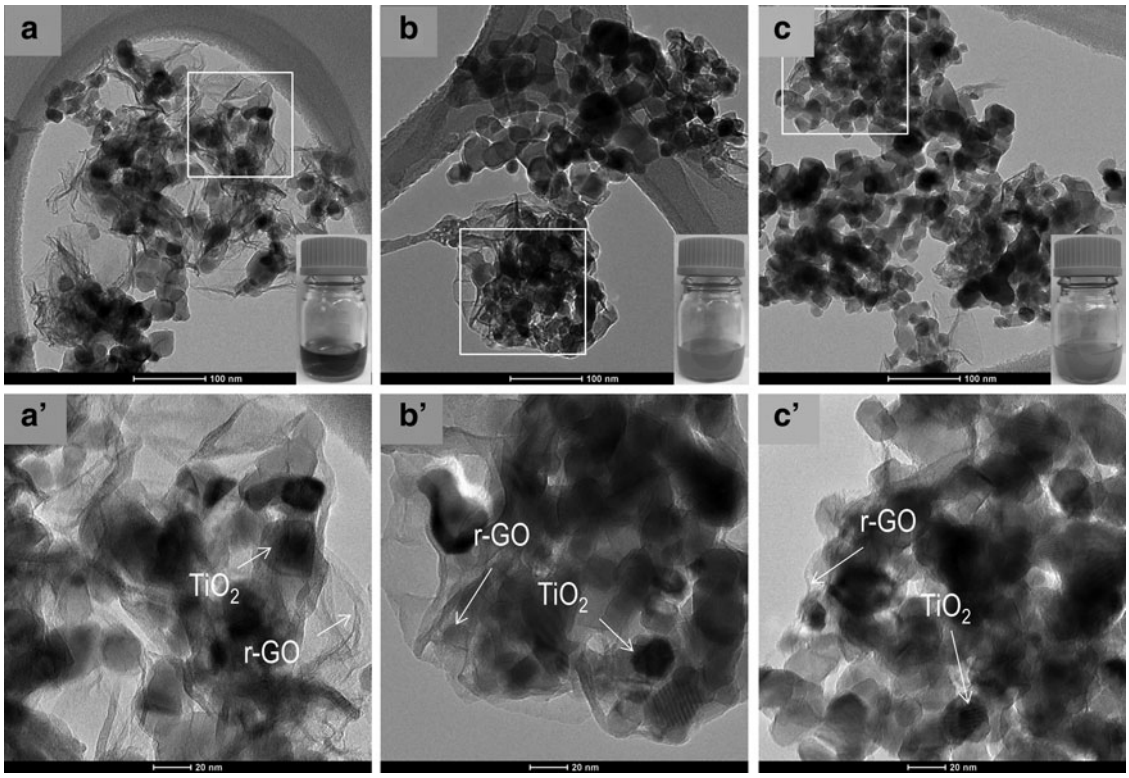

FIG. 2. Transmission electron microscopy (TEM) images of reduced graphene oxide (rGO)–titania (TiO_2) nanocomposites with different TiO_2 weight percentages: **(a)** 5 wt%; **(b)** 10 wt%, and **(c)** 20 wt%. **(a′–c′)** Magnified TEM images from the selected areas (indicated by the white squares) in **(a–c)**. The photo of each precursor was also inserted in the corresponding image.

was equipped with a PLOT capillary column (Supelco Carboxen-1010) and a thermal conductivity detector. To rule out the possibility of carbon contamination in the system, a series of blank tests were performed under N_2 atmosphere (without using CO_2 as the source gas), with CO/CH_4 detection and CO_2 evolution from the nanocomposites with different TiO_2 loadings prepared at various synthesis temperatures.

Results and Discussion

As mentioned earlier, the precursors for the described nanocomposites were made by mixing GO nanosheets and TiO_2 NPs in DI water at predetermined ratios. The as-prepared mixtures were then characterized by the DLS method to get information of particle size and zeta potential, and the results are summarized in Table 1. From the table, the hydrodynamic size was found to increase significantly with TiO_2 percentages, indicating the agglomeration of the two components. This is due to the electrostatic interaction between TiO_2 NPs and GO nanosheets, as both of them carry charges. This is also confirmed by the fact that the zeta potential of the mixture slightly decreases with an increase in TiO_2 percentage, which could be considered a result of partial neutralization. It is also seen from Table 1 that the polydispersity index fluctuates when the TiO_2 percentage increases, indicating the decreased stability of the mixture. However, the absolute values of the zeta potentials are still high enough to ensure the stability of the mixture for several days.

The precursor was then used for preparation of the GO-TiO_2 nanocomposites by the FuAR method. Typical TEM images of the nanocomposites with different TiO_2 percentages, that is, 5, 10, and 20 wt%, are shown in Fig. 2. It is apparent that most TiO_2 NPs were encapsulated well within the crumpled GO structure when the TiO_2 content was low (e.g., 5 wt%; Fig. 2a). More free TiO_2 NPs were found outside the crumpled rGO structure when the percentage increased. In the case of 20 wt% TiO_2, TiO_2 NPs are mostly observed while the GO nanosheets are almost not visible (Fig. 2c). As shown in Table 1 and from our previous research (Wang *et al.*, 2012b), the size of the GO nanosheets is around several 100 nm. It implies that only a certain fraction (upper limit) of TiO_2 NPs could be encapsulated into the crumpled ball. To avoid the interference of free TiO_2 NPs in the structure, nanocomposites with 5 wt% TiO_2 were prepared at different temperatures from 200°C to 1000°C, to investigate the thermal impact on the nanocomposites, in particular the thermal reduction ratios of these nanocomposites, which could significantly influence the subsequent CO_2 photoreduction efficiency.

The rGO-TiO_2 nanocomposites were then subjected to CO_2 photoreduction analysis in the flow reactor as shown in Fig. 1b. To ensure that there is no carbon contamination in the system, two samples with different TiO_2 loadings (1 and 5 wt%) prepared at 800°C were irradiated by the Xe lamp for 8 h by using N_2, instead of CO_2, as the source gas. The results are plotted in Supplementary Figure S1; neither CO nor CH_4 was detected, indicating that the system is free of carbon contamination. In addition, CO_2 evolution of the rGO-TiO_2 samples prepared at lower synthesis temperatures (200°C, 400°C, and 500°C) was also investigated under an N_2 atmosphere. As demonstrated in Supplementary Fig. S2, an increase in CO_2 concentration for some samples was observed due to the removal of functional groups from the GO surfaces. However, the maximum CO_2 concentration was only about 3% of the baseline of CO_2 flow (3 mL/min). Further, no CO_2 photoreduction product (i.e., CO or CH_4) was observed for these samples. This indicates that the CO_2 generated from the simultaneous photoreduction of GO nanosheets negligibly contributed to CO_2 photoreduction. Therefore, any reduction product in the subsequent photoreduction analyses should be from the CO_2 source gas that was converted by the photocatalysts.

The CO_2 photoreduction results for nanocomposites synthesized with different TiO_2 percentages and at different temperatures are plotted in Fig. 3. In most cases, CO_2 was successfully reduced to CO based on the typical two electron-two proton reaction mechanism ($CO_2 + 2e^- + 2H^+ \rightarrow CO + H_2O$) (Wang *et al.*, 2012b). Figure 3a shows the CO yield as a function of TiO_2 percentages, where the optimal CO yield was achieved at 5 wt% TiO_2 loading. Lower conversion

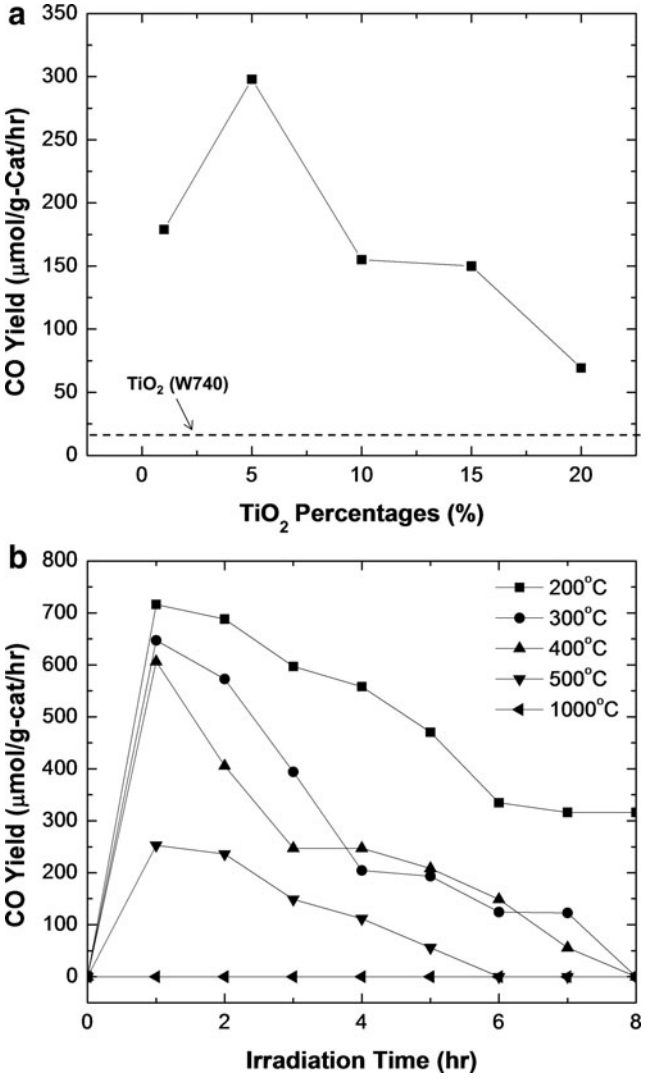

FIG. 3. CO_2 photoreduction analysis of rGO-TiO_2 nanocomposites prepared at different conditions. **(a)** Different TiO_2 weight percentages at 800°C. **(b)** Different synthesis temperatures with the same TiO_2 weight percentage (5 wt%). The irradiation time was fixed at 8 h for all analyses.

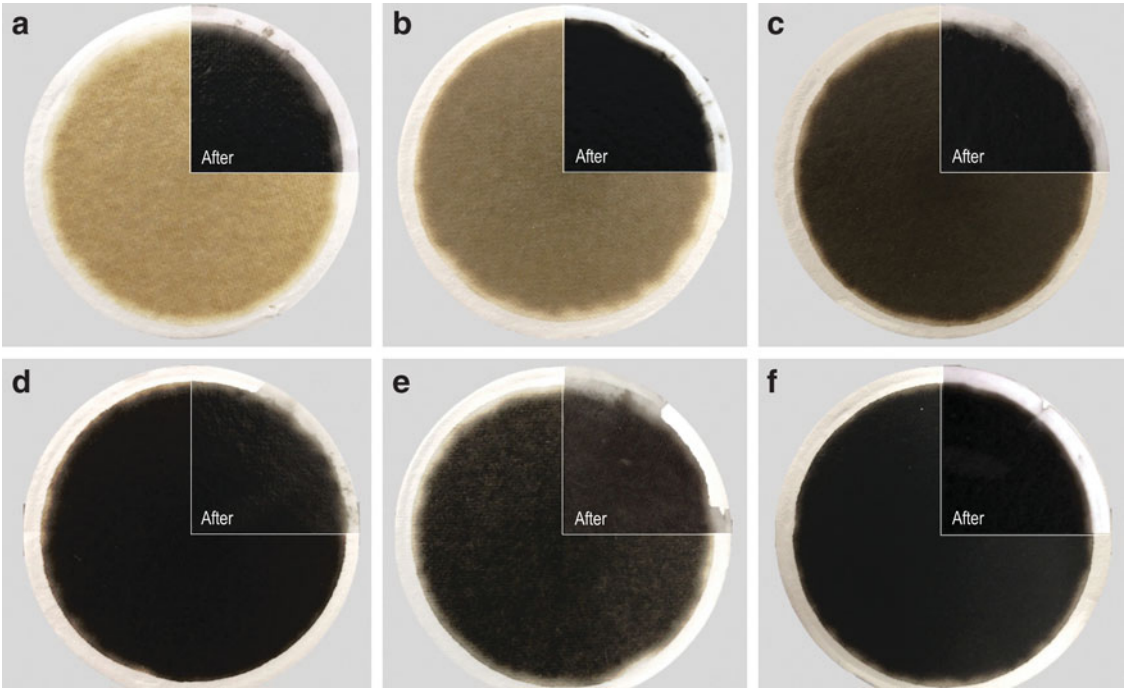

FIG. 4. Color change of rGO-TiO_2 nanocomposites prepared at different temperatures before and after CO_2 photoreduction analysis: **(a)** 200°C, **(b)** 300°C, **(c)** 400°C, **(d)** 500°C, **(e)** 800°C, and **(f)** 1000°C.

efficiency was achieved at a lower TiO_2 percentage, such as 1 wt%, possibly due to less active catalysts available for photoreduction. After reaching the optimal performance at 5 wt%, the CO yield, however, decreases gradually with an increase in TiO_2 loading. This is because the increased TiO_2 percentage could increase the possibility of more free TiO_2 NPs outside the rGO nanosheets as indicated in Fig. 2. Without direct contact with the rGO nanosheets, the e^-–h^+ lifetime could not be improved as expected. For a 20 wt% TiO_2 sample, the CO yield is very close to that of pristine TiO_2 NPs. This could be also attributed to the interparticle e^-–h^+ recombination, which could significantly decrease the CO_2 photoreduction performance. CO_2 photoreduction results of nanocomposites prepared at 200–1000°C are shown in Fig. 3b. From the figure, it is apparent that nanocomposites prepared at 200°C have the highest CO yield (716 μmol/g-cat per hour). The performance monotonically decreased with an increase in temperature. The sample prepared at 1000°C has almost no function at all. The results suggest that synthesis temperature played an important role in tailoring rGO surface functionality and electron trapping capability, and hence the enhanced CO_2 photoreduction performance.

It is obvious that the GO nanosheets are reduced to rGO by thermally removing surface functional groups. This is evident from the color of the samples as indicated in the pictures in Fig. 4. At 200°C, the nanocomposites are yellowish (Fig. 4a). The color turned dark brown when the temperature increased to 300°C, and became even darker at 400°C and higher. Black color was observed for the sample prepared at 1000°C, indicating a substantial removal of the surface groups.

It has been well documented that the conductivity of rGO is much lower than that of pure graphene, as the surface defects created due to the removal of functional groups

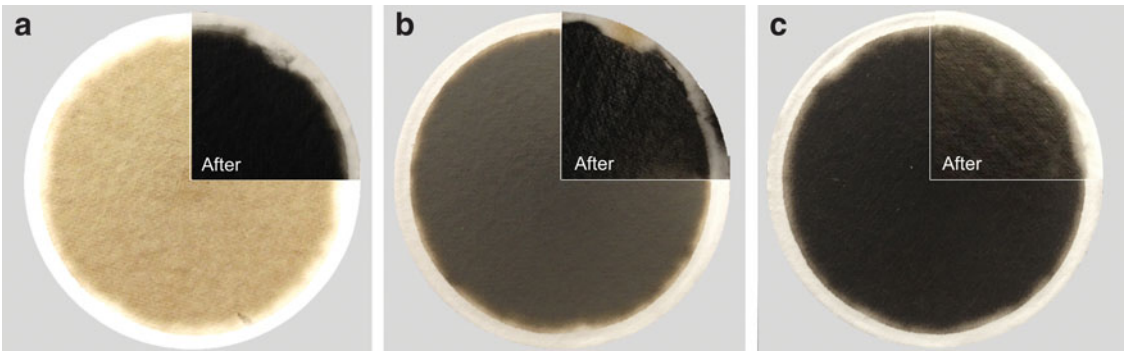

FIG. 5. Color change of rGO-TiO_2 nanocomposites prepared at different temperatures before and after photoreduction analysis under nitrogen: **(a)** 200°C, **(b)** 400°C, and **(c)** 500°C.

hindered the charge transfer inside graphene structure (Kamat, 2010, 2011; Ding *et al.*, 2011). This is particularly true for the case of thermal reduction where more surface defects could be created due to violent reactions occurring during thermal removal of surface functional groups, which results in lower conductivity. This could explain why a lower performance was achieved for nanocomposites prepared at higher synthesis temperatures. Meanwhile, an interesting phenomenon of color change after photoreduction was observed. As from Fig. 4, the color of all samples became black after CO_2 photoreduction, which implies that the photoreduction of GO to rGO may happen simultaneously with CO_2 photoreduction (Kamat, 2010, 2011; Ding *et al.*, 2011).

To test our hypothesis, the CO_2 gas was changed to N_2 and the three rGO-TiO_2 nanocomposites (5 wt% TiO_2) prepared at different temperatures were illuminated. The same color change was observed as shown in Fig. 5. All samples turned black after irradiation for 8 h, implying that TiO_2 could photoreduce GO nanosheets into rGO. As shown in Supplementary Fig. S2, CO_2 evolution was observed but no CO was found from these samples. The simultaneous photoreduction is a softer method as compared with thermal reduction, resulting in less damage and improved performance in conductivity (Ding *et al.*, 2011). Compared with the samples obtained at higher temperatures, the samples prepared at lower temperatures preserved more functional groups and had less surface defects due to thermal reduction. These functional groups were photoreduced and formed rGO, leaving softer surface defects and hence improved electronic conductivity.

To verify the surface characteristics of the samples, the nanocomposites before and after CO_2 photoreduction were analyzed by Raman spectroscopy, a powerful nondestructive tool to characterize the changes brought about in the electronic structure of GO (Das *et al.*, 2008a, 2008b). Three samples prepared at different temperatures were used, that is, 200, 400, and 800°C. The Raman spectra of these nanocomposites are plotted in Fig. 6. The peaks at 400–650 cm^{-1} (Liu *et al.*, 2013) can be assigned to TiO_2 anatase phase. D and G bands are clearly observed at around 1348 and 1583 cm^{-1}, respectively (Marchand *et al.*, 1982), suggesting that the structure of GO is maintained in the nanocomposites. A small peak at about 2700 cm^{-1} is also detectable for all three samples, which can be attributed to the 2D band (Das *et al.*, 2008a). The intensities of the Raman spectra of the three samples were normalized at the G band for a comparison of the D/G band ratio. Before photoreduction, it is obvious that 200 and 400°C samples have almost the same spectra and the D and G bands are relatively broad with D/G ratios of 0.967 and 0.987, respectively. The two peaks became more defined at 800°C and the D/G band ratio decreased to 0.924. The decreased D/G ratio indicates the decreased surface functional groups on the rGO surface due to thermal reduction (Marchand *et al.*, 1982; Liu *et al.*, 2013). The same three samples were used for photoreduction by TiO_2 NPs as mentioned earlier. The samples prepared at 200 and 400°C demonstrated obvious changes in D band intensity as shown in Fig. 6b. The D/G band ratios of the two samples increased to 1.163 and 1.083, respectively. This is possibly due to the presence of dangling bonds of the sp^2 carbon or soft defects created due to photoreduction (Zhang *et al.*, 2013), as more surface functional groups were presented in the lower

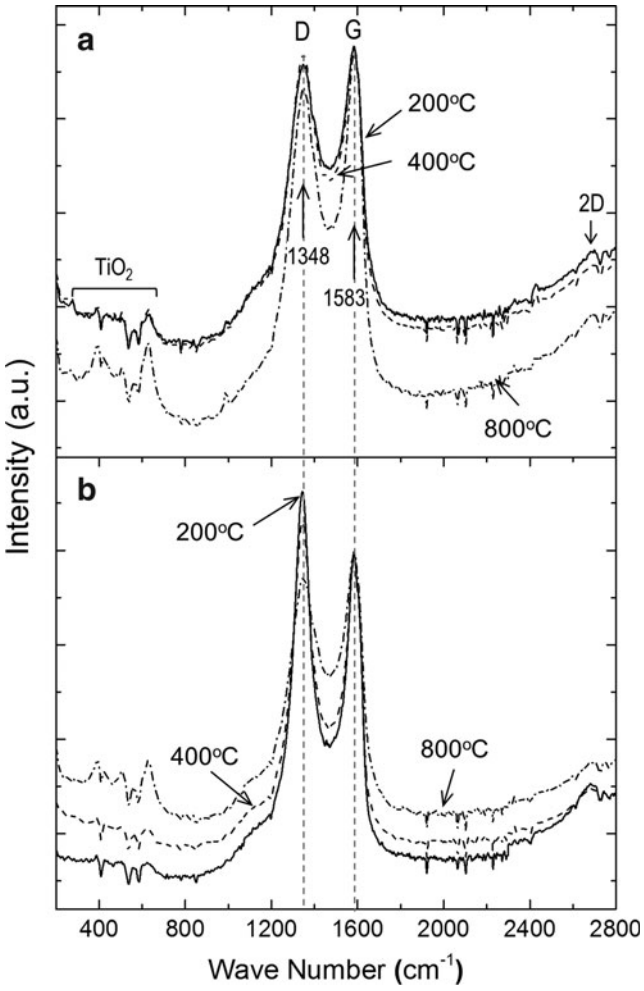

FIG. 6. Raman spectra of rGO-TiO_2 nanocomposites prepared at different temperatures before **(a)** and after CO_2 photoreduction analysis **(b)**. TiO_2 percentage was fixed at 5 wt%.

temperature samples. Both D and G peaks become more defined than those in the 800°C sample, suggesting that the GO has been photocatalytically reduced to rGO and possibly possesses better electronic properties. The 800°C sample did not show obvious changes after photoreduction (D/G ratio = 0.938), indicating that the thermal reduction has completely removed its surface functional groups. The defects created due to thermal reduction are permanently present in the structure, which may adversely affect the charge transfer and hence the photocatalytic performance.

Conclusions

rGO-TiO_2 nanocomposites were prepared by a single-step aerosol technique. Effects of synthesis temperature and TiO_2 percentage were investigated systematically. An optimal TiO_2 percentage of 5 wt% was achieved with a maximal CO yield of more than 700 μmol/g-cat/h, which is much higher than that of pristine TiO_2 due to the enhanced electron-trapping capability of rGO nanosheets. Nanocomposites synthesized at a lower temperature demonstrate better performance, which indicates that simultaneous photoreduction of GO nanosheets in the CO_2 photoreduction process contributes to the enhancement of the CO_2 photoreduction

performance. It should also be noted that the preparation of these nanocomposites was realized by means of a single-step aerosol method, requiring much less time and energy as compared with traditional thermal or chemical processes. The continuous and scalable manner of this process also ensures the mass production of these nanocomposites for industrial applications.

Acknowledgments

This work was supported by funds from the Lopata Endowment at Washington University in St. Louis. Partial support from the Consortium for Clean Coal Utilization at Washington University in St. Louis is gratefully acknowledged. Electron microscopy work was performed at the Nano Research Facility (NRF) at Washington University in St. Louis, a member of the National Nanotechnology Infrastructure Network (NNIN), supported by the National Science Foundation under Grant no. ECS-0335765.

Author Disclosure Statement

No competing financial interests exist.

References

Biswas, P., Wang, W.N., and An, W.J. (2011). The energy-environment nexus: Aerosol science and technology enabling solutions. *Front. Env. Sci. Eng. China* 5, 299.

Das, A., Pisana, S., Chakraborty, B., Piscanec, S., Saha, S.K., Waghmare, U.V., Novoselov, K.S., Krishnamurthy, H.R., Geim, A.K., Ferrari, A.C., and Sood, A.K. (2008a). Monitoring dopants by Raman scattering in an electrochemically top-gated graphene transistor. *Nat. Nanotechnol*. 3, 210.

Das, B., Voggu, R., Rout, C.S., and Rao, C.N.R. (2008b). Changes in the electronic structure and properties of graphene induced by molecular charge-transfer. *Chem. Commun*. 41, 5155.

Ding, Y.H., Zhang, P., Zhuo, Q., Ren, H.M., Yang, Z.M., and Jiang, Y. (2011). A green approach to the synthesis of reduced graphene oxide nanosheets under UV irradiation. *Nanotechnology* 22, 215601.

Eckstein, H., and Kreibig, U. (1993). Light-induced aggregation of metal-clusters. *Z. Phys. D*. 26, 239.

Fujishima, A., Zhang, X.T., and Tryk, D.A. (2008). TiO_2 photocatalysis and related surface phenomena. *Surf. Sci. Rep*. 63, 515.

Hummers, W.S. (1958). Preparation of graphitic oxide. *J. Am. Chem. Soc*. 80, 1339.

Indrakanti, V.P., Kubicki, J.D., and Schobert, H.H. (2009). Photoinduced activation of CO_2 on Ti-based heterogeneous catalysts: Current state, chemical physics-based insights and outlook. *Energy Environ. Sci*. 2, 745.

ISO 13321 (1996). *Particle Size Analysis—Photon Correlation Spectroscopy*, Section 2.2. Geneva, Switzerland: International Organization for Standarization.

Kamat, P.V. (2010). Graphene-based nanoarchitectures. Anchoring semiconductor and metal nanoparticles on a two-dimensional carbon support. *J. Phys. Chem. Lett*. 1, 520.

Kamat, P.V. (2011). Graphene-based nanoassemblies for energy conversion. *J. Phys. Chem. Lett*. 2, 242.

Kimura, K. (1994). Photoenhanced van der Waals attractive force of small metallic particles. *J. Phys. Chem.* 98, 11997.

Liu, Y.J., Aizawa, M., Peng, W.Q., Wang, Z.M., and Hirotsu, T. (2013). Carbon nanosheet-titania nanocrystal composites from reassembling of exfoliated graphene oxide layers with colloidal titania nanoparticles. *J. Solid State Chem*. 197, 329.

Luo, J.Y., Jang, H.D., Sun, T., Xiao, L., He, Z., Katsoulidis, A.P., Kanatzidis, M.G., Gibson, J.M., and Huang, J.X. (2011). Compression and aggregation-resistant particles of crumpled soft sheets. *ACS Nano* 5, 8943.

Ma, X.F., Zachariah, M.R., and Zangmeister, C.D. (2012). Crumpled nanopaper from graphene oxide. *Nano Lett*. 12, 486.

Marchand, A., Lespade, P., and Couzi, M. (1982). Characterization of carbon-carbon composites by Raman microprobe. I. Studies on graphitization. *Carbon* 20, 149.

Metz, B., Davidson, O., de Coninck, H., Loos, M., and Meyer, C. (2005). *IPCC Special Report on Carbon Dioxide Capture and Storage*. New York: Cambridge University Press.

Song, C.S. (2006). Global challenges and strategies for control, conversion and utilization of CO_2 for sustainable development involving energy, catalysis, adsorption and chemical processing. *Catal. Today* 115, 2.

Stankovich, S., Dikin, D.A., Dommett, G.H.B., Kohlhaas, K.M., Zimney, E.J., Stach, E.A., Piner, R.D., Nguyen, S.T., and Ruoff, R.S. (2006). Graphene-based composite materials. *Nature* 442, 282.

Tseng, I.H., Wu, J.C.S., and Chou, H.Y. (2004). Effects of sol-gel procedures on the photocatalysis of Cu/TiO_2 in CO_2 photoreduction. *J. Catal*. 221, 432.

Usubharatana, P., McMartin, D., Veawab, A., and Tontiwachwuthikul, P. (2006). Photocatalytic process for CO_2 emission reduction from industrial flue gas streams. *Ind. Eng. Chem. Res*. 45, 2558.

Wang, W.N., An, W.J., Ramalingam, B., Mukherjee, S., Niedzwiedzki, D.M., Gangopadhyay, S., and Biswas, P. (2012a). Size and structure matter: Enhanced CO_2 photoreduction efficiency by size-resolved ultrafine Pt nanoparticles on TiO_2 single crystals. *J. Am. Chem. Soc*. 134, 11276.

Wang, W.N., Jiang, Y., and Biswas, P. (2012b). Evaporation-induced crumpling of graphene oxide nanosheets in aerosolized droplets: confinement force relationship. *J. Phys. Chem. Lett*. 3, 3228.

Wang, W.N., Park, J., and Biswas, P. (2011). Rapid synthesis of nanostructured $Cu\text{-}TiO_2\text{-}SiO_2$ composites for CO_2 photoreduction by evaporation driven self-assembly. *Catal. Sci. Technol*. 1, 593.

Zhang, J., Huang, Z.H., Xu, Y., and Kang, F.Y. (2013). Hydrothermal synthesis of graphene/Bi_2WO_6 composite with high adsorptivity and photoactivity for azo dyes. *J. Am. Ceram. Soc*. 96, 1562.